Simulation of Active Cardiac Dynamics with Orthotropic Hyperelastic Material Model

Release 1.00

Ken C. L. Wong[1], Linwei Wang[1], Heye Zhang[2], Huafeng Liu[3], and Pengcheng Shi[1]

May 21, 2008

[1]B. Thomas Golisano College of Computing and Information Sciences, Rochester Institute of Technology, Rochester, New York, USA
Email: {kenclwong, maomaowlw}@mail.rit.edu, pengcheng.shi@rit.edu
[2]Bioengineering Institute, University of Auckland, New Zealand
Email: heye.zhang@auckland.ac.nz
[3]State Key Laboratory of Modern Optical Instrumentation, Zhejiang University, Hanzhou, China
Email: liuhf@zju.edu.cn

Abstract

Meaningful physical models are important for studying cardiac physiology, such as quantitative assessments of pathology via changes in model parameters, and recovering information from medical images. In order to achieve realistic deformation studies, an anatomically accurate cardiac model under the prolate spheroidal coordinate system has been proposed, which comprises the pole-zero constitutive law characterized by 18 material parameters. Nevertheless, the large number of parameters and the complicated mathematics under the curvilinear coordinate system make it difficult to implement and computationally expensive. In consequence, we propose a cardiac model under the cartesian coordinate system comprising the Costa law, which is tailored for medical image analysis. The Costa law is characterized by a strain energy function with only seven material parameters, but has been reported as the best among the five tested well-known models in a comparative study, including the pole-zero law. In our framework, the penalty method for material incompressibility is used to avoid introduction of extra variables. Furthermore, we introduce a simple but novel boundary condition for enforcing cardiac specific boundary displacements under the cartesian coordinate system. With the active stresses provided by cardiac electromechanical models, and also the blood pressures acting as the natural boundary conditions on the endocardial surfaces, the physiologically plausible active deformation of the heart can be simulated. Experiments have been done on a cubical object to verify the correctness of the implementation, and also on a canine heart architecture to show the physiological plausibility of the cardiac model.

Contents

1 Introduction

Physiologically meaningful cardiac models are important for studying cardiac physiology, such as quantitative assessments in pathology study via changes in model parameters, and recovering information from medical images [7]. At macroscopic level, an active cardiac deformation model comprises an electrical propagation model, an electromechanical coupling model, and also a biomechanical model, among which the biomechanical model plays the crucial role in archiving realistic deformation. In [10] and [12], a cardiac electromechanical model has been introduced for image analysis and simulation. The model utilizes the Mooney-Rivlin material model, which is an isotropic hyperelastic material model usually used to describe the behavior of incompressible rubber like material [5]. With the implementation under the cartesian coordinate system, this framework is relatively easy to implement and computationally efficient. Nevertheless, according to biomechanical literatures [3, 4, 6], apart from nonlinear stress-strain relation and incompressibility, the myocardial tissues are also locally orthotropic in nature because of their fibrous-sheet structures, thus using an isotropic model will effect the physiological meaningfulness of the active cardiac deformation. On the other hand, an anatomically accurate cardiac model was proposed in [9] with more realistic material properties. This model comprises a nonlinear orthotropic pole-zero strain energy function characterized by 18 material parameters, which is implemented under the prolate spheroidal coordinate system so that the heart geometry can be best expressed. In consequence, this model provides physiologically plausible deformation. However, the large number of material parameters increases the difficulties of the derivation of the elasticity tensor. Furthermore, some complicated mathematical terms which only appear in the curvilinear coordinate system, such as the contravariant components, make this framework theoretically very hard to implement and also computationally expensive. Moreover, the transformations between the local (cartesian), global (curvilinear), and element coordinate systems also impose large difficulties in implementation and scalability, especially for image analysis where data are presented in the cartesian coordinate system.

In view of these problems, we introduce a cardiac model targeting for medical image analysis. It comprises an orthotropic hyperelastic material model, and is implemented under the cartesian coordinate system, thus it can be physiologically plausible yet relatively easy to implement. The Costa law is utilized as the biomechanical constitutive law, which consists a nonlinear strain energy function containing only seven material parameters, but is reported as the best among the five tested well-known constitutive laws in a comparative study, including the pole-zero law [2, 11]. The penalty method for material incompressibility is used to avoid introduction of hydrostatic pressures as extra variables. Furthermore, a simple but novel boundary

conditions for enforcing cardiac specific boundary displacements under the cartesian coordinate system is introduced. With the active stresses provided by electromechanical models, and also the blood pressures acting as the natural boundary conditions on the endocardial surfaces, the physiologically plausible active deformation of the heart can be simulated. In the best of our knowledge, we are the first one to implement the Costa law up to the ventricular level. Experiments have been done on a cubical object to verify the correctness of the implementation, and on a canine heart architecture to show the physiological plausibility of the proposed cardiac model.

2 Methodology

The biomechanically accurate material model, the incompressibility of the myocardium, and also the cardiac specific boundary conditions are essential for realistic cardiac deformation. With the cardiac system dynamics connecting these components with the kinematic quantities and active contraction forces, physiologically plausible deformations of the heart can then be achieved.

2.1 Hyperelastic Material Model

Biomechanical experiments showed that material properties of the myocardium are nonlinear and orthotropic, thus the fibrous-sheet structure and also the nonlinear stress-strain relation have to be properly considered [3, 4, 6].

Strain Energy Function

There are different hyperelastic material models describing the nonlinear myocardial stress-strain relation [9, 2, 11]. In an experiment of constitutive parameter optimizations with pig cardiac tissues, the Costa law has been reported as the best among the five well-known nonlinear constitutive laws [2, 11]. Furthermore, compared with the pole-zero law that has 18 parameters [9], the Costa law has only seven parameters, which results in a much smaller degree of freedoms for material parameters recovery from medical images, and thus can largely improve the computational efficiency especially when statistical state-space frameworks are utilized [13, 16]. As our goal is to construct a cardiac model which can facilitate medical image analysis, the Costa law is chosen as our material model, which describes the local orthotropic material property through the strain energy function [2]:

$$\Psi(E_{ff},E_{fn},E_{fs},E_{nf},E_{nn},E_{ns},E_{sf},E_{sn},E_{ss}) = \frac{1}{2}a(e^{Q}-1) \tag{1}$$

where

$$\begin{aligned} Q =& b_{ff}E_{ff}^2 + 2b_{fn}\left(\frac{1}{2}(E_{fn}+E_{nf})\right)^2 + 2b_{fs}\left(\frac{1}{2}(E_{fs}+E_{sf})\right)^2 \\ &+ b_{nn}E_{nn}^2 + 2b_{ns}\left(\frac{1}{2}(E_{ns}+E_{sn})\right)^2 + b_{ss}E_{ss}^2 \end{aligned} \tag{2}$$

with $E_{\alpha\beta}$ the components of the Green-Lagrange strain tensor $\mathbf{E}$ defined under the local coordinate system (f,n,s; fiber, normal, sheet). a, b_{ff}, b_{fn}, b_{fs}, b_{nn}, b_{ns} and b_{ss} are the seven constitutive material parameters of the tissue, with the unit of a as Pa and $b_{\alpha\beta}$ have no unit. The f-n-s coordinate system represents the local fibrous-sheet structure, which orientation can be different at different locations.

Stress Tensor

With the strain energy function defined, we can derive the second Piola-Kirchhoff (PKII) stress tensor $\mathbf{S} = \partial\Psi/\partial\mathbf{E}$ under the f-n-s basis as [5]:

$$S_{\alpha\beta} = \frac{\partial\Psi}{\partial E_{\alpha\beta}} = \begin{cases} ae^{Q}b_{\alpha\beta}E_{\alpha\beta}, & \text{if } \alpha = \beta \\ \frac{1}{2}ae^{Q}b_{\alpha\beta}(E_{\alpha\beta} + E_{\beta\alpha}), & \text{if } \alpha \neq \beta, \text{with } b_{\alpha\beta} = b_{\beta\alpha} \end{cases} \tag{3}$$

It can be seen that the stress-strain relation is highly nonlinear, and the material stiffness increases with the deformation.

Elasticity Tensor

The problems of finite elasticity are nonlinear and usually have no closed-form solution, thus incremental solution techniques of Newton's type are required. In consequence, the elasticity tensor $\mathbb{C}$ which provides the linearized stress-strain relation at a particular stain state is given as [5]:

$$\mathbb{C} = \frac{\partial\mathbf{S}}{\partial\mathbf{E}} = \frac{\partial^2\Psi}{\partial\mathbf{E}\partial\mathbf{E}} \quad \text{or} \quad C_{\alpha\beta rs} = \frac{\partial^2\Psi}{\partial E_{\alpha\beta}\partial E_{rs}} \tag{4}$$

$\mathbb{C}$ possesses the major symmetries ($C_{\alpha\beta rs} = C_{rs\alpha\beta}$) and the minor symmetries ($C_{\alpha\beta rs} = C_{\beta\alpha rs} = C_{\alpha\beta sr}$), thus it has only 21 independent components.

Defining $[\Delta\mathbf{S}]_{\text{local}} = [\Delta S_{ff}, \Delta S_{nn}, \Delta S_{ss}, \Delta S_{fn}, \Delta S_{fs}, \Delta S_{ns}]^{\mathrm{T}}$ and $[\Delta\mathbf{E}]_{\text{local}} = [\Delta E_{ff}, \Delta E_{nn}, \Delta E_{ss}, 2\Delta E_{fn}, 2\Delta E_{fs}, 2\Delta E_{ns}]^{\mathrm{T}}$, with ΔS_{ij} and ΔE_{ij} the components of the local incremental PKII stress and strain tensors respectively, we have $[\Delta\mathbf{S}]_{\text{local}} = [\mathbb{C}]_{\text{local}}[\Delta\mathbf{E}]_{\text{local}}$, where:

$$[\mathbb{C}]_{\text{local}} = \begin{bmatrix} C_{ffff} & C_{ffnn} & C_{ffss} & C_{fffn} & C_{fffs} & C_{ffns} \\ C_{nnff} & C_{nnnn} & C_{nnss} & C_{nnfn} & C_{nnfs} & C_{nnns} \\ C_{ssff} & C_{ssnn} & C_{ssss} & C_{ssfn} & C_{ssfs} & C_{ssns} \\ C_{fnff} & C_{fnnn} & C_{fnss} & C_{fnfn} & C_{fnfs} & C_{fnns} \\ C_{fsff} & C_{fsnn} & C_{fsss} & C_{fsfn} & C_{fsfs} & C_{fsns} \\ C_{nsff} & C_{nsnn} & C_{nsss} & C_{nsfn} & C_{nsfs} & C_{nsns} \end{bmatrix} \tag{5}$$

This matrix is symmetric because $\mathbb{C}$ possesses the major symmetries. Note that $[\mathbb{C}]_{\text{local}}$ must be multiplied with incremental *engineering* shear strain components ($2\Delta E_{ij}, i \neq j$) to obtain the proper incremental PKII stress tensor components.

To transform $[\mathbb{C}]_{\text{local}}$ into the global coordinate system, we have the relation:

$$[\mathbb{C}]_{\text{global}} = [T][\mathbb{C}]_{\text{local}}[R][T]^{-1}[R]^{-1} \tag{6}$$

with $[T]$ the transformation matrix which is a function of the f-n-s directions, and $[R]$ is a diagonal matrix responsible for the transformation between strain and engineering strain components, with elements $\{1,1,1,2,2,2\}$. As both local and global coordinate systems are cartesian in our model, $[T]$ is much simpler compared with those using curvilinear global coordinate system [9].

2.2 Penalty Method for Incompressibility

It has been widely accepted in literatures that the myocardium is nearly incompressible [3, 4, 6]. In order to approximate this condition while not increasing the number of variables, the penalty method is used, which

is based on the idea of modeling the nearly incompressibility by using a large value of bulk modulus [5]. It is standard to use the decoupled representation of the strain-energy function:

$$\Psi(\mathbf{E}) = \Psi_{\text{vol}}(J) + \Psi_{\text{iso}}(\overline{\mathbf{E}}) \quad \text{with} \quad \Psi_{\text{vol}}(J) = \kappa \mathcal{G}(J) \tag{7}$$

where $J = (\det \mathbf{C})^{1/2}$ defining the volume ratio, with $\mathbf{C}$ the right Cauchy-Green tensor, and $\overline{\mathbf{E}} = 0.5(J^{-2/3}\mathbf{C} - \mathbf{I})$. Ψ_{vol} describes the volumetric elastic response, and Ψ_{iso} describes the isochoric elastic response of the hyperelastic material which has the same form of (1) with $\mathbf{E}$ replaced by $\overline{\mathbf{E}}$.

The volumetric contribution Ψ_{vol} is characterized by a penalty parameter $\kappa > 0$, which is an adjustable numerical parameter chosen through numerical experiments. The function $\mathcal{G}$ is known as the penalty function with the form:

$$\mathcal{G}(J) = \frac{1}{2}(J-1)^2 \tag{8}$$

With (7) and (8), the respective PKII stress tensor can now be defined as:

$$\mathbf{S} = \mathbf{S}_{\text{vol}} + \mathbf{S}_{\text{iso}} = Jp\mathbf{C}^{-1} + \frac{\partial \Psi_{\text{iso}}}{\partial \mathbf{E}}; \;\; p = \frac{\mathrm{d}\Psi_{\text{vol}}}{\mathrm{d}J} = \kappa(J-1) \tag{9}$$

and the respective decoupled representation of elasticity tensor is given as:

$$\mathbb{C} = \mathbb{C}_{\text{vol}} + \mathbb{C}_{\text{iso}} = \frac{\partial \mathbf{S}_{\text{iso}}}{\partial \mathbf{E}} + \frac{\partial \mathbf{S}_{\text{vol}}}{\partial \mathbf{E}} \tag{10}$$

Although this approach cannot impose total incompressibility, it can avoid the introduction of hydrostatic pressures which may lead to a global system matrix with rank deficiency [5].

2.3 Enforcing Cardiac Specific Displacement Boundary Conditions

Various structures constraining the cardiac deformation, among which the pericardial sac exhibiting high axial stiffness and low transmural shear resistance plays an important role in limiting the movement of the epicardium [9]. It is relatively easy to simulate this boundary condition under the prolate spheroidal coordinate system by limiting the corresponding displacement variables, however, it is not trivial under the cartesian coordinate system. To simulate the axial stiffness, we propose the boundary condition:

$$\mathbf{u} \cdot \mathbf{n} = b \tag{11}$$

where $\mathbf{u}$ and $\mathbf{n}$ are the displacement and normal on the epicardial surface under the cartesian coordinate system. b controls the displacement along the normal direction, which can be a function of deformation, or zero if displacement is forbidden. This boundary condition can be imposed using the generalized Lagrange multiplier or penalty method on the epicardium [1]. Furthermore, the penalty method is used to impose the transmural shear resistance for avoiding excessive displacement along the epicardial surface. This boundary enforcement method is important for medical image analysis as it provides an efficient yet realistic way to couple the model with information from images, that is, to incorporate the displacement information of the epicardium extracted from the images into b. Although (11) is simple, we could not find any relevant literature which specifies this simple but important relation for simulating the constraint of the pericardial sac under the cartesian coordinate system. The experimental results in section 3.2 will show that this constraint leads to the proper twisting motion of the myocardium.

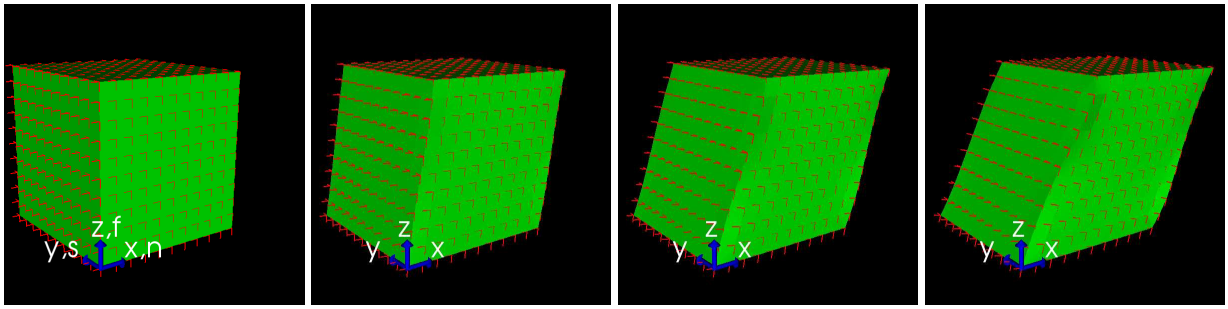

(a)

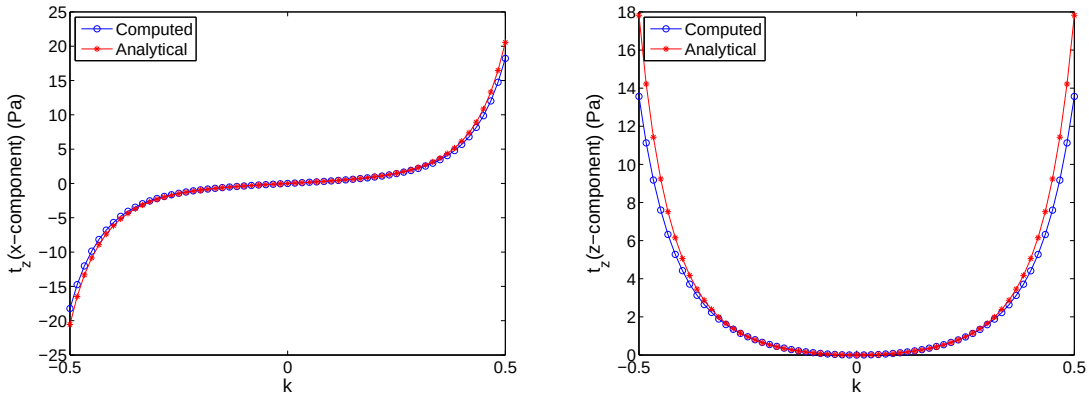

(b)

Figure 1: Static shear test on a cubical object. (a) The bottom surface is fixed and displacement is enforced along the x-direction on the top surface. Red lines indicate the fiber-normal-sheet orientations. Left to right: $k = 0, 0.167, 0.334$, and 0.5. (b) Analytical and computed forces on the positive z-surface (top surface) of the cubical object. Left: the x-component. Right: the z-component.

2.4 Cardiac System Dynamics under Finite Deformation

The cardiac system dynamics acts as the central link between the material properties, external forces, and kinematic quantities. The displacement-based total-Lagrangian (TL) system dynamics of the heart under finite deformation is utilized, whose matrix representation is given as [16]:

$$\mathbf{M}\ddot{\mathbf{U}} + \mathbf{C}\dot{\mathbf{U}} + \mathbf{K}\Delta\mathbf{U} = \mathbf{R}_c + \mathbf{R}_b - \mathbf{R}_i \tag{12}$$

where $\mathbf{M}$ is the mass matrix, $\mathbf{C}$ is the damping matrix, and $\mathbf{K}$ is the strain incremental stiffness matrix containing the material and deformation properties. The hyperelastic material properties and incompressibility is embedded in $\mathbf{K}$ as it comprises $\mathbb{C}$ in (10). $\mathbf{R}_c$ is the force vector containing the active forces obtained through a electromechanical coupling model. $\mathbf{R}_b$ is the force vector for enforcing boundary conditions, and $\mathbf{R}_i$ is the nodal force vector for finite deformation only and is related to the internal stresses. $\ddot{\mathbf{U}}$, $\dot{\mathbf{U}}$ and $\Delta\mathbf{U}$ are the respective nodal acceleration, velocity and incremental displacement vectors. By using the Newmark method for temporal integration, (12) can be solved for the nodal kinematic quantities, and thus the active cardiac deformation can be obtained.

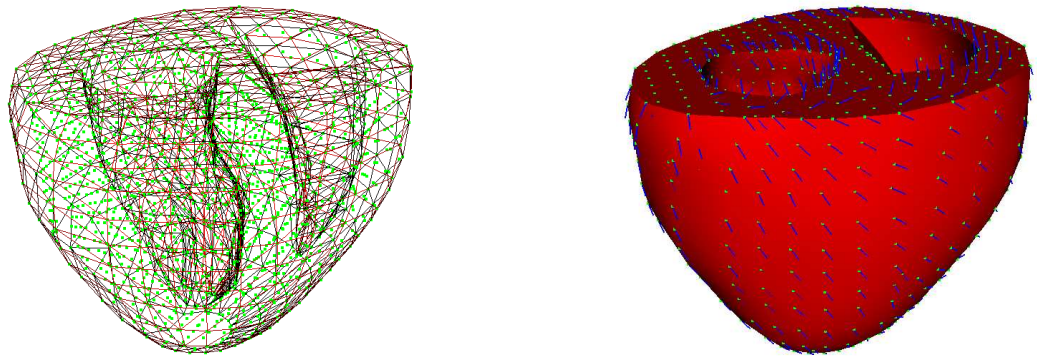

(a) (b)

Figure 2: Meshfree representation constructed from the canine heart architecture. (a) A set of nodes (green) bounded by surface elements (red lines) representing the cardiac boundaries. (b) Fiber orientations shown as blue lines on the heart surfaces.

3 Experiments

3.1 Cubical Object

In order to verify the correctness of the implementation, a static passive shear test described in [11] was adopted. A cubical object with lengths 60 mm is utilized, which has the initial fibrous-sheet structure *f*-*n*-*s* pointing towards the *z*-*x*-*y* axes of the cartesian coordinate system. Suppose we have the deformation gradient tensor in the global *x*-*y*-*z* coordinate system as:

$$\mathbf{F} = \begin{bmatrix} 1 & 0 & k \\ 0 & 1 & 0 \\ 0 & 0 & 1 \end{bmatrix}_{x,y,z} \Rightarrow \mathbf{E} = \frac{1}{2} \begin{bmatrix} 0 & 0 & k \\ 0 & 0 & 0 \\ k & 0 & k^2 \end{bmatrix}_{x,y,z} \tag{13}$$

where k ranges between -0.5 and 0.5. Then the analytical force on the surface with normal pointing towards the positive z-direction (positive z-surface) is:

$$t_z = \begin{bmatrix} \frac{1}{2}Aak(b_{ff}k^2 + b_{fn})e^Q \\ 0 \\ A\frac{1}{2}ak^2 b_{ff}e^Q \end{bmatrix} \tag{14}$$

with A the area of the surface before deformation, and $Q = 0.25b_{ff}k^4 + 0.5b_{fn}k^2$.

In the experiment, displacement boundary conditions are enforced on both z-surfaces of the cubical object to simulate the deformation in (13) in 60 steps, and the force on the positive z-surface is computed. Figure 1(a) shows the deformed structures. In Figure 1(b), we can see that the computed results are very close to the analytical results, yet the errors increase when the deformation becomes large. This is because for the hyperelastic material, the stress-strain relation is very steep when the strain is large, and thus the linearization error of the elasticity tensor becomes large when the step size is constant. The y-component of the computed force is about 10^{-5} of the x and z-components. These show that our implementation can capture the realistic stress-strain relation of the Costa law.

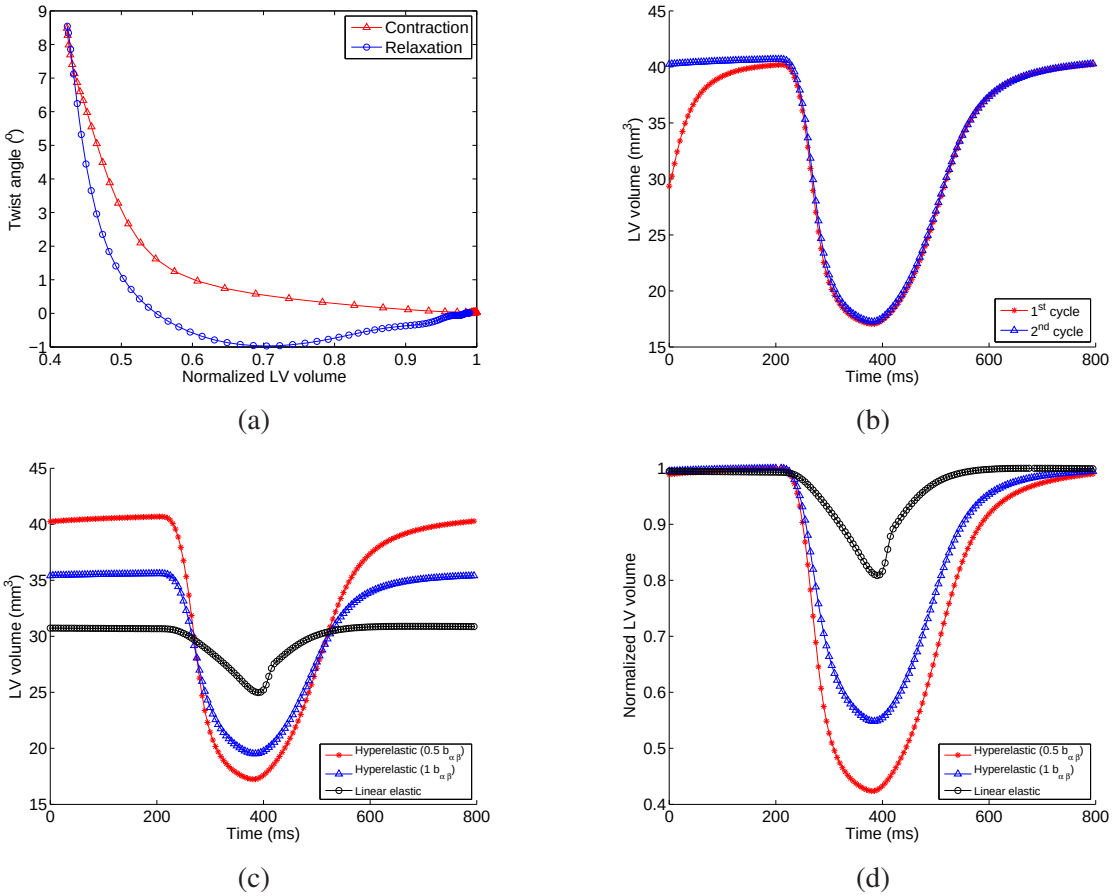

Figure 3: (a) Averaged twist angle versus normalized LV volume. The positive twist angle represents anticlockwise rotation, when viewed along the long axis of LV from the apex. (b) LV volume change versus time of different cardiac cycles for the 0.5 $b_{\alpha\beta}$ case. (c) LV volume change versus time of different material parameters. (d) Normalized LV volume change of (c), for easier comparison of the stroke volumes. Stroke volumes of the 0.5 $b_{\alpha\beta}$, 1 $b_{\alpha\beta}$, and linear elastic cases are 57.6%, 45.2%, and 19.1% respectively.

3.2 Canine Heart Architecture

The canine heart architecture of the University of Auckland was used, which provides both the geometry and fibrous-sheet structure [9]. A meshfree representation was constructed from the canine heart geometry [8], with the fiber orientations shown in Figure 2. Active contraction forces were simulated through the cardiac electromechanical model described in [16], and deformations of one cardiac cycle in 800 ms were computed. As the canine heart architecture was obtained through in-vitro anatomical experiments when the bloods were not inside the ventricles, its geometry should not be treated as the end-of-diastole, and blood pressures were applied to the surfaces of the endocardia of the left and right ventricles (LV and RV) to inflate them. This step built up stresses in the myocardium at the end of diastole, and thus increase the physiological meaningfulness of the simulation. Two consecutive cardiac cycles were run so that the effects of the improper initial conditions, such as the zero velocities, zero accelerations, and zero myocardial stresses, could be alleviated. Figure 3(b) shows the change of the LV volume of the two cardiac cycles, and we can see that the end-of-diastole volume become stable in the second cycle.

Figure 4 shows the deformation of the simulated beating heart, and also a MRI sequence for comparison. The

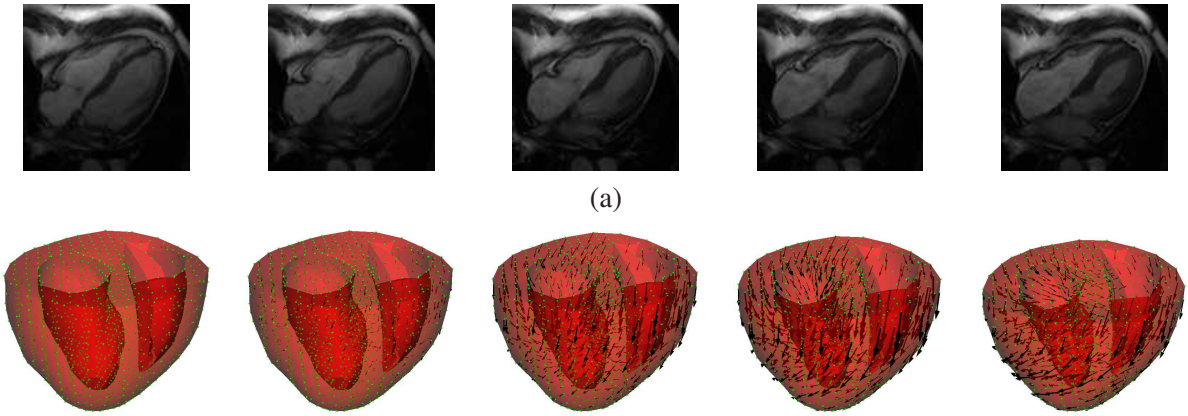

(a)

(b)

Figure 4: Deformations of cardiac geometries during systole. (a) MRI sequence of a healthy human heart. Left to right: 0 ms, 86 ms, 172 ms, 258 ms, and 344 ms. (b) Simulated cardiac cycle. The green dots represent the material points in the myocardium and the black arrows represent the incremental displacement vectors. Left to right: 220 ms, 240 ms, 260 ms, 280 ms, and 300 ms.

MRI sequence contains 20 frames of a cardiac cycle of a healthy human. Each 3D image frame contains eight image slices, with 10 mm inter-slice spacing, in-plane resolution of 1.56 mm/voxel, and temporal resolution of 43 ms/frame. It can be seen from the MRI that, because of the constraint of the pericardial sac, the motion of the epicardium along the normal direction of the epicardial surface is limited. Furthermore, the apex is almost fixed, and the base moves towards the apex during contraction. All of these deformation patterns can be found in our simulation because we have applied proper displacement boundary conditions to simulate the effects of the structures surrounding the heart, especially those described in section 2.3. If the boundary condition of the pericardial sac is not included, the epicardium will displace towards the septum and results in unrealistic deformation. We can also observe from the displacement vectors of Figure 4(b) that the heart twisted during contraction. Again, because of the boundary conditions described in section 2.3, the amounts and directions of the twist angles are similar to those described in the literatures [4, 9], with the numerical results plotted in Figure 3(a).

The values of the material parameters were adopted from [11] for the initial experiments ($a = 0.171$ kPa, $b_{ff} = 34, b_{fn} = 11.1, b_{fs} = 12.6, b_{nn} = 19.3, b_{ns} = 9.01, b_{ss} = 13$). Nevertheless, even when very large contraction stresses were applied (around 50 kPa), the stroke volume of LV, which is defined as the difference between the end-diastole volume and the end-systole volume, could not achieve a proper value which should be about 60-70% when normalized by the end-diastole volume. This is because the stiffness of the material exponentially increases with the deformation, and the myocardium becomes too stiff to contract any more. As stated in [2], the material parameters are actually different at different locations of the heart, and some locations are softer so that larger deformation is allowed. As the precise distribution of different material parameters is not available, in order to investigate the effect of the parameters to the stroke volume, we performed another simulation with all the $b_{\alpha\beta}$ halved. Larger stroke volume was obtained, and the temporal changes of the LV volume became more similar to those presented in literatures [4, 6](Figure 3(c) and (d)). Furthermore, in order to verify the importance of using hyperelastic material, a simulation using linear elastic material was performed under exactly the same setting, with Young's moduli along and cross the myofiber as 75 and 25 kPa respectively [4]. It can be seen that the resulted stroke volume is very small, and the change of volume is almost linear compared with the hyperelastic model. This is because the stiffness of the linear elastic material does not change with deformation, while the hyperelastic material is relatively

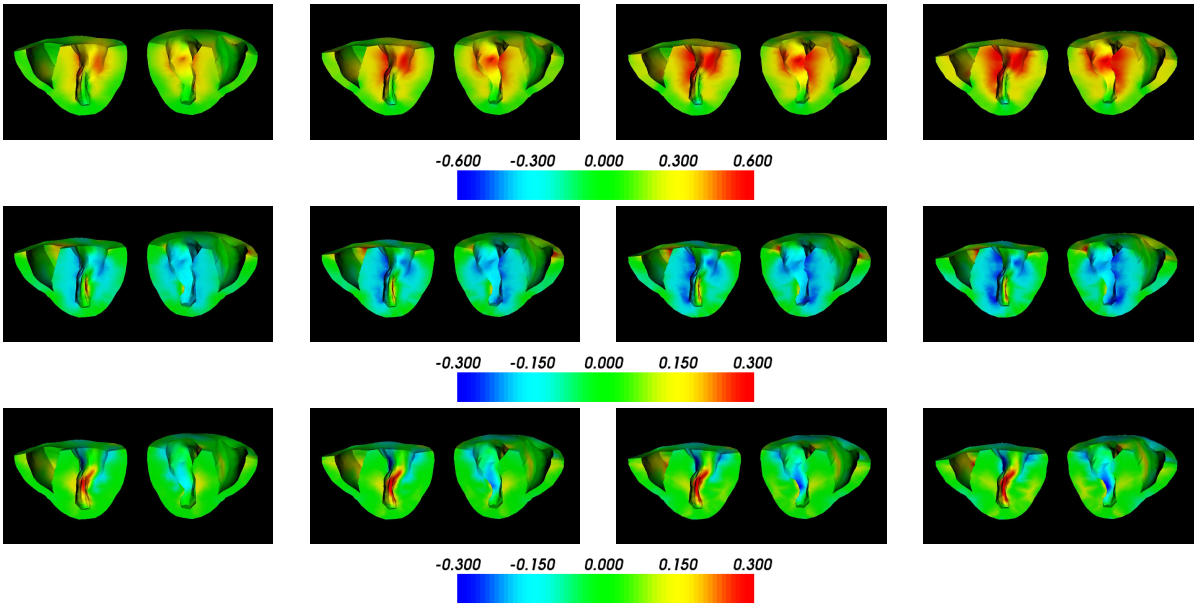

Figure 5: Strain maps of the simulated cardiac cycle. Top to bottom: radial, circumferential, and radial-circumferential strains, defined under a cylindrical coordinate system with the long axis of the LV as the long axis. Left to right: 300 ms, 320 ms, 340 ms, and 360 ms (during systole). Positive values represent extensions and negative values represent contractions.

soft at the beginning and becomes very stiff after deformation.

The strain maps of the simulation with 0.5 $b_{\alpha\beta}$ are shown in Figure 5. While the displacements were obtained under the cartesian coordinate system, the strains were represented under the cylindrical coordinate system for the physiological meaningfulness. From Figure 5, we can observe the circumferential contraction and radial extension of the myocardium during systole, which are consistent with the descriptions in cardiological literatures [4, 6].

4 Conclusion and Discussion

In this paper, we have introduced a cardiac model tailored for medical image analysis. The Costa Law which was verified as the best among the five tested well-known hyperelastic material models has been adopted, its relatively few material parameters can facilitate the efficiency of the material property recovery from medical images. The corresponding PKII stress tensor and elasticity tensor have been derived, and the penalty method for incompressibility has been presented. We have also proposed a simple but realistic displacement boundary condition to simulate the constraint of the pericardial sac under the cartesian coordinate system. The correctness of the implementation was verified through an experiment on a cubical object, and the physiological plausibility of our model was verified through experiments on a canine heart architecture.

As we can enforce blood pressures as the natural boundary conditions to inflate LV and RV, our model is capable of incorporating the four cardiac phases of blood filling, isovolumic contraction, blood ejection, and isovolumic relaxation. While the blood filling and the blood ejection phases can be described through physical models such as the Windkessel model [14], the isovolumic phases can only be handled numerically without proper physical meaning [10, 12]. In view of this, only the blood filling phase is included into our

current cardiac model, and we are working on using the computational fluid dynamics to provide proper stress boundary conditions for the isovolumic phases, or even other phases. Furthermore, this cardiac model will be used for cardiac information recovery from medical images after completion. As this model is highly nonlinear, following the spirit of [15], the unscented Kalman filter will be utilized for the recovery process.

References

[1] K. J. Bathe. *Finite Element Procedures*. Prentice Hall, 1996. 2.3

[2] K. D. Costa, J. W. Holmes, and A. D. McCulloch. Modelling cardiac mechanical properties in three dimensions. *Philos. Trans. R. Soc. London*, 359(1783):1233–1250, 2001. 1, 2.1, 3.2

[3] Y. C. Fung. *Biomechanics: Mechanical Properties of Living Tissues*. Springer-Verlag, 2nd edition, 1993. 1, 2.1, 2.2

[4] L. Glass, P. Hunter, and A. McCulloch, editors. *Theory of Heart: Biomechanics, Biophysics, and Nonlinear Dynamics of Cardiac Function*. Springer-Verlag, 1991. 1, 2.1, 2.2, 3.2, 3.2

[5] G. A. Holzapfel. *Nonlinear solid mechanics: a continuum approach for engineering*. John Wiley & Sons, Inc., 2000. 1, 2.1, 2.1, 2.2, 2.2

[6] J. D. Humphrey. *Cardiovascular solid mechanics: cells, tissues, and organs*. Springer-Verlag, 2001. 1, 2.1, 2.2, 3.2

[7] P. J. Hunter. Modeling human physiology: The IUPS/EMBS physiome projec. *Proceedings of the IEEE*, 94(4):678–691, 2006. 1

[8] H. Liu and P. Shi. Meshfree particle method. In *IEEE International Conference on Computer Vision*, pages 289–296, 2003. 3.2

[9] M. Nash. *Mechanics and Material Properties of the Heart using an Anatomically Accurate Mathematical Model*. PhD thesis, University of Auckland, 1998. 1, 2.1, 2.1, 2.3, 3.2, 3.2

[10] J. Sainte-Marie, D. Chapelle, R. Cimrman, and M. Sorine. Modeling and estimation of the cardiac electromechanical activity. *Computers and Structures*, 84:1743–1759, 2006. 1, 4

[11] H. Schmid, M. P. Nash, A. A. Young, and P. J. Hunter. Myocardial material parameter estimation — a comparative study for simple shear. *Journal of Biomechanical Engineering*, 128:742–750, 2006. 1, 2.1, 3.1, 3.2

[12] M. Sermesant, P. Moireau, O. Camara, J. Sainte-Marie, R. Andriantsimiavona, R. Cimrman, D. L. G. Hill, D. Chapelle, and R. Razavi. Cardiac function estimation from MRI using a heart model and data assimilation: advances and difficulties. *Medical Image Analysis*, 10:642–656, 2006. 1, 4

[13] P. Shi and H. Liu. Stochastic finite element framework for simultaneous estimation of cardiac kinematic functions and material parameters. *Medical Image Analysis*, 7:445–464, 2003. 2.1

[14] J.-J. Wang, A. B. O'Brien, N. G. Shrive, K. H. Parker, and J. V. Tyberg. Time-domain representation of ventricular-arterial coupling as a windkessel and wave system. *Am J Physiol Heart Circ Physiol*, 284:H1358–H1368, 2003. 4

[15] L. Wang, H. Zhang, P. Shi, and H. Liu. Imaging of 3D cardiac electrical activity: A model-based recovery framework. In *International Conference on Medical Image Computing and Computer Assisted Intervention*, volume 4190 of *LNCS*, pages 792–799. Springer, 2006. 4

[16] K. C. L. Wong, H. Zhang, H. Liu, and P. Shi. Physiome-model-based state-space framework for cardiac deformation recovery. *Academic Radiology*, 14(11):1341–1349, 2007. 2.1, 2.4, 3.2